Electronic Supplementary Information (ESI)

Accelerated electrochemical nitrate-to-ammonia conversion over bimetallic Ni_2Mo_3N with mechanistic insights

So Eun Jang,[a] Jae Young Kim*[b] and Duck Hyun Youn*[a]

[a]*Department of Chemical Engineering, Department of Integrative Engineering for Hydrogen Safety, Kangwon Nation University, Chuncheon 24341, South Korea.*

[b]*Korea Research Institute of Chemical Technology, Daejeon 34114, South Korea.*

*Corresponding authors

E-mail address: youndh@kangwon.ac.kr, jaeykim@krict.re.kr

Determination of ion concentration

Determination of NO_3^- :

Firstly, a certain volume of electrolyte was taken out from the electrolytic cell and diluted to 5 mL to detection range. Then, 0.1 mL of 1 M HCl was added into the aforementioned solution. After 5 minutes, the absorbance was measured by UV-Vis spectrophotometer at a wavelength of 220 nm. The concentration-absorbance curve was calibrated using a series of standard sodium nitrate solutions.

Determination of NO_2^- :

The concentration of nitrite was analyzed using the typical Griess method. A mixture of p-aminobenzenesulfonamide (4.0 g), N-(1-Naphthyl) ethylenediamine dihydrochloride (0.2 g), ultrapure water (50 mL) and phosphoric acid (10 mL) was used as the color reagent. A certain volume of electrolyte was taken out from the electrolytic cell and diluted to 5 mL to detection range. Then, 0.1 mL color reagent was added into the aforementioned 5 mL sample and mixed uniformly. After 20 minutes, the absorbance at 540 nm was measured by UV-Vis spectrophotometer. The concentration-absorbance curve was calibrated using a series of standard sodium nitrite solutions.

Determination of NH_3 :

The concentration of ammonia was determined using Nessler's reagent method. First, a certain volume of electrolyte was taken out from the electrolytic cell and diluted to 5 ml to detection range. Then, 0.1 mL potassium sodium tartrate solution and 0.1 mL Nessler's reagent were added into the above 5 mL sample and mixed uniformly. After 20 minutes, the absorbance at 420 nm was measured by UV-Vis spectrophotometer. The concentration-absorbance curve was calibrated using a series of standard ammonium chloride solutions.

^{15}N isotope labeling experiments :

Isotope labeling experiments were performed using $Na^{15}NO_3$-^{15}N as a nitrogen source to confirm the origin of generated ammonia. After chronoamperometry tests, 20 mL of the electrolyte was taken out and the pH value was adjusted to be weak acid with HCl. After that, the adjusted electrolyte was concentrated to about 3 mL via rotary evaporator. 950 μL of the condensed solution was mixed with 50 mL of DMSO-d_6. The mixed solution was analyzed using ^{1}H NMR (600 MHz). $^{14}NH_4Cl$ and $^{15}NH_4Cl$ solutions were measured to obtain the standard triplet and doublet peaks, following the same procedure.

In situ Raman Spectroscopy measurements:

A JASCO NRS-4500 Raman spectrometer with a laser at an excitation wavelength of 532 nm was used for in situ analysis. A Pt wire and Ag/AgCl (3 M KCl) electrode was used as the counter electrode and the reference electrode, respectively. The electrolyte consisted of 0.1 M KOH with 0.1 M NaNO3 (30 mL). CV was conducted in advance at a scan rate of 50 mV s^{-1} until steady-state polarization curves were obtained. Raman spectra were collected at applied potentials ranging from +0.2 V to –0.8 V, with each potential held for 120 s under potentiostatic control.

On-line Differential Electrochemical Mass Spectrometry (DEMS) measurements :

Hiden Analytical HPR-20 R&D analyser was used for on-line DEMS measurements. Ni_2Mo_3N/NF, Pt wire, and Ag/AgCl (3 M KCl) electrodes were used as working, counter and reference electrodes, respectively. Prior to measurements, the electrolyte (0.1 M KOH with 0.1 M $NaNO_3$) was purged with Ar gas for 30 min to remove dissolved O_2. Cyclic voltammetry (CV) was conducted until steady-state polarization curves were achieved, using a scan rate of 50 mV s^{-1}. And chronoamperometry tests were conducted for 300 s at constant potential after the baseline kept steady. Then, the corresponding mass signals were collected. After the electrochemical test was over and the mass signal returned to baseline, the next cycle was started. After four cycles, the DEMS test was completed.

Calculation of the yield and Faradaic efficiency

The ammonia yield rate (mg h^{-1} cm^{-2}) was calculated by the Eq. (1) :

$$\text{Yield} = \frac{C_{NH3} \times V}{m_{NH3} \times t \times A} \quad (1)$$

The Faradaic efficiency (FE) was calculated by the Eq. (2), (3), and (4) :

$$FE_{NH3} = \frac{8 \times F \times C_{NH3} \times V}{m_{NH3} \times Q} \times 100\ \% \quad (2)$$

$$FE_{NO2} = \frac{2 \times F \times C_{NO2} \times V}{m_{NO2} \times Q} \times 100\ \% \quad (3)$$

$$FE_{H2} = \frac{2 \times F \times n_{H2}}{Q} \times 100\ \% \quad (4)$$

where C_{NH3} is the measured ammonia concentration (mg L^{-1}), C_{NO2} is the measured nitrite concentration (mg L^{-1}), V is the volume of electrolyte (30 mL), m_{NH3} is the molar mass of ammonia, m_{NO2} is the molar mass of nitrite, t is the electrolysis time (1 h), A is the area of the working electrode (1 x 1 cm^2), n is the molar amount of H_2. F is faradaic constant (96485 C mol^{-1}), Q is the total charge passing the electrode.

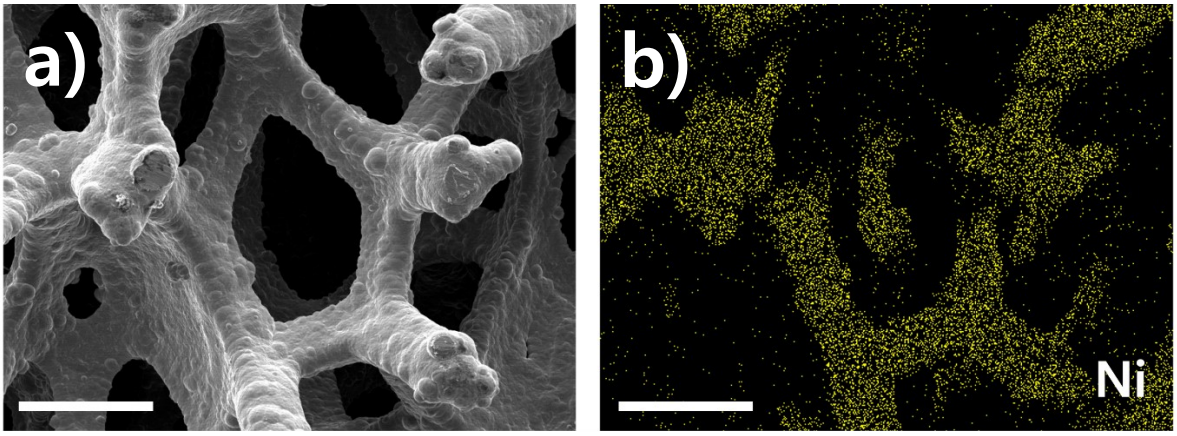

Fig. S1. (a) SEM image of Ni foam and corresponding EDS mapping image of (b) Ni. Scale bars denote 200 μm.

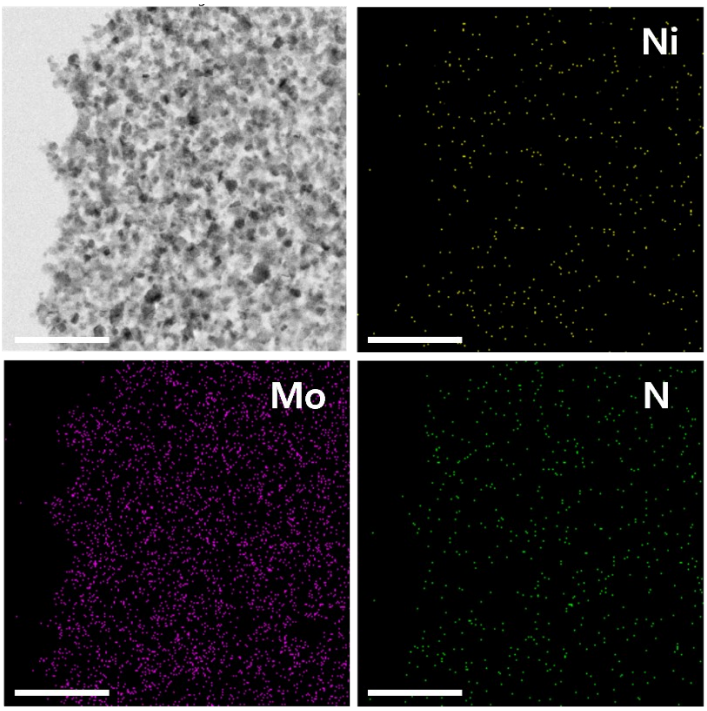

Fig. S2. TEM-EDS mapping images of Ni, Mo, and N for Ni_2Mo_3N/NF. Scale bar denotes 100 nm.

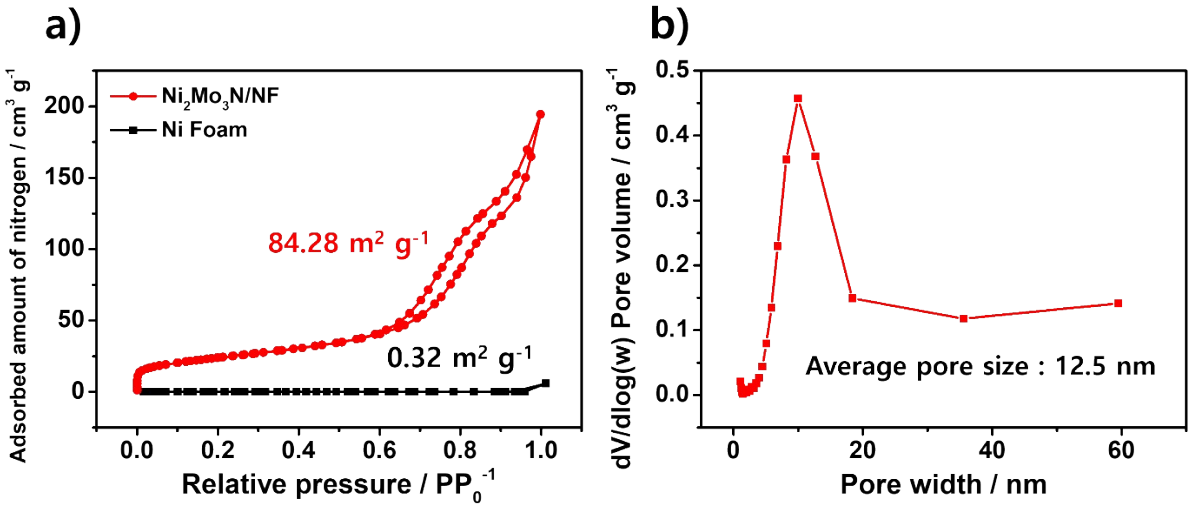

Fig. S3. (a) N_2 adsorption-desorption isotherms for Ni_2Mo_3N/NF and Ni foam, (b) pore size distribution of Ni_2Mo_3N/NF.

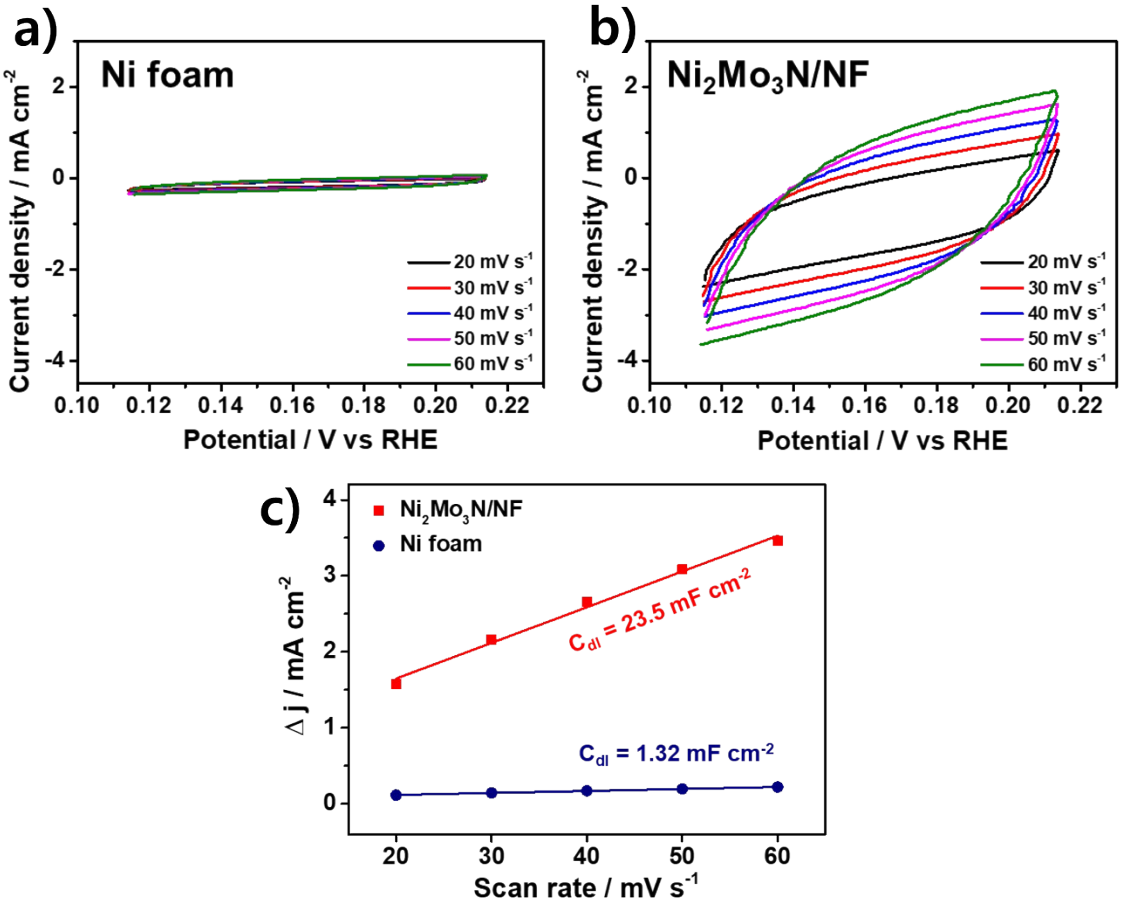

Fig. S4. Cyclic voltammograms of (a) Ni foam and (b) Ni_2Mo_3N/NF at different scan rates. (c) Measured capacitive current as a function of scan rate of Ni_2Mo_3N/NF, and Ni foam.

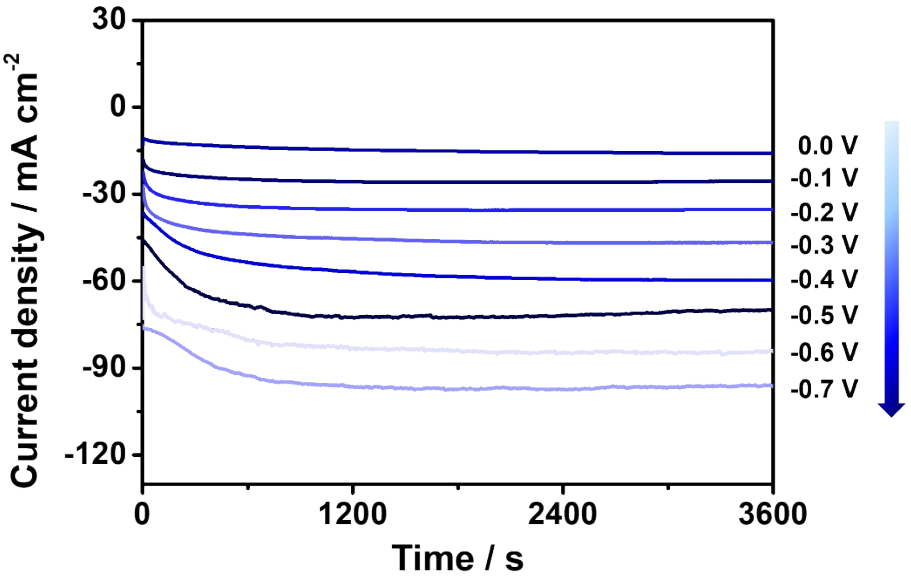

Fig. S5. Chronoamperometry curves of Ni_2Mo_3N/NF at different potentials for 1 h in 0.1 M KOH with 0.1 M $NaNO_3$ electrolyte.

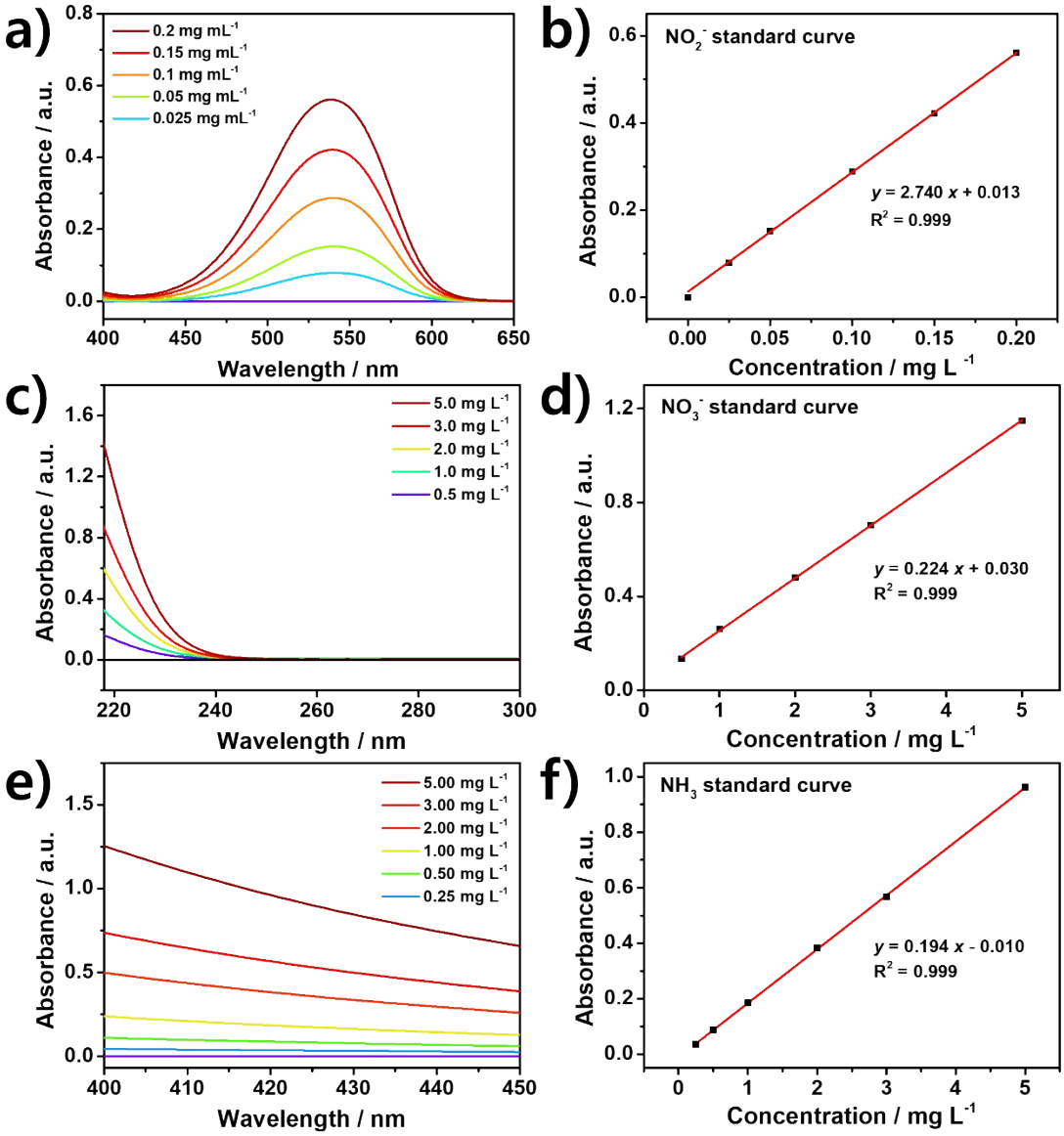

Fig. S6. a) UV-vis adsorption spectra and b) calibration curves for NO_2^-. c) UV-vis adsorption spectra and d) calibration curves for NO_3^-. e) UV-vis adsorption spectra and f) calibration curves for NH_3.

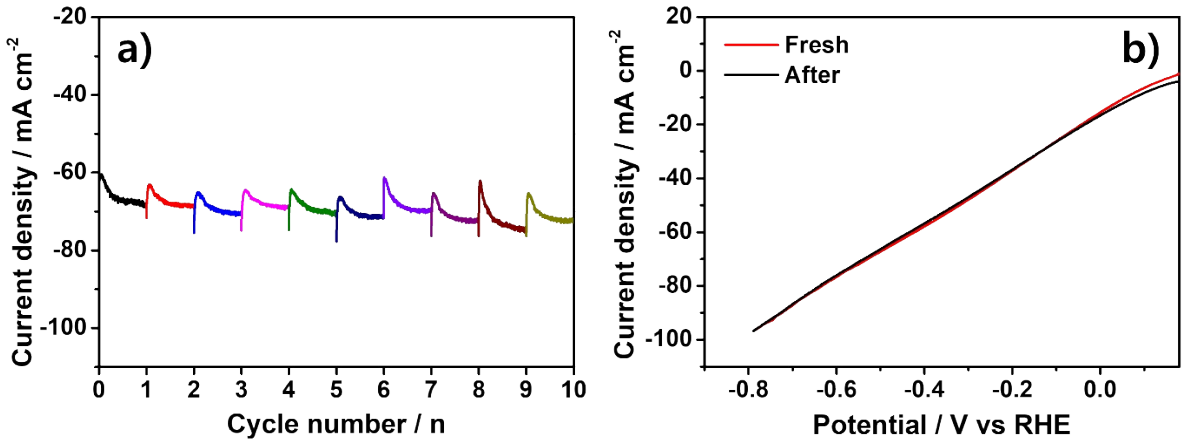

Fig. S7. (a) Consecutive cycling tests of Ni_2Mo_3N/NF at -0.5 V vs RHE for NO_3^-RR. (b) LSV curves of Ni_2Mo_3N/NF fresh and after cycling tests.

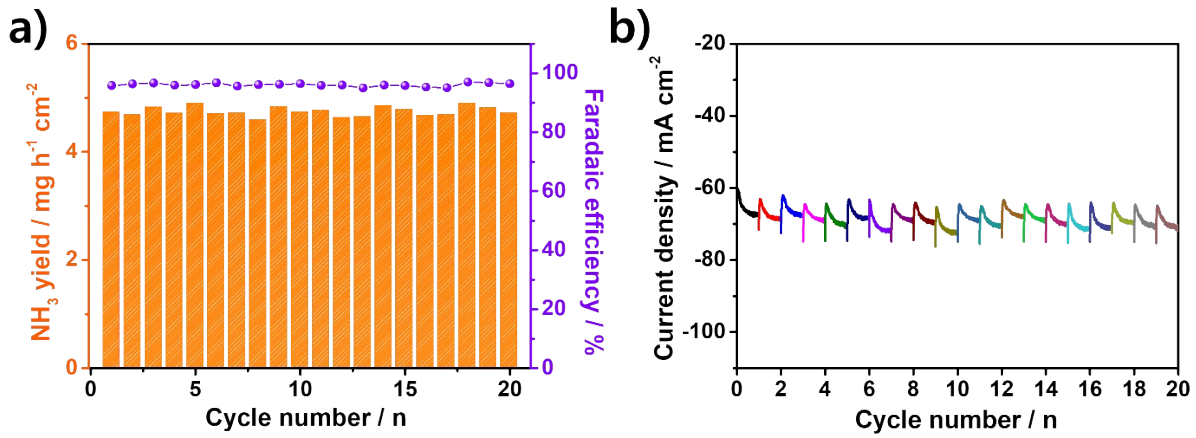

Fig. S8. Consecutive 20 cycling test of Ni_2Mo_3N/NF at -0.5 V vs RHE. (a) FE_{NH3} and NH_3 yield and (b) the chronoamperometry curves during 20 cycling stability test.

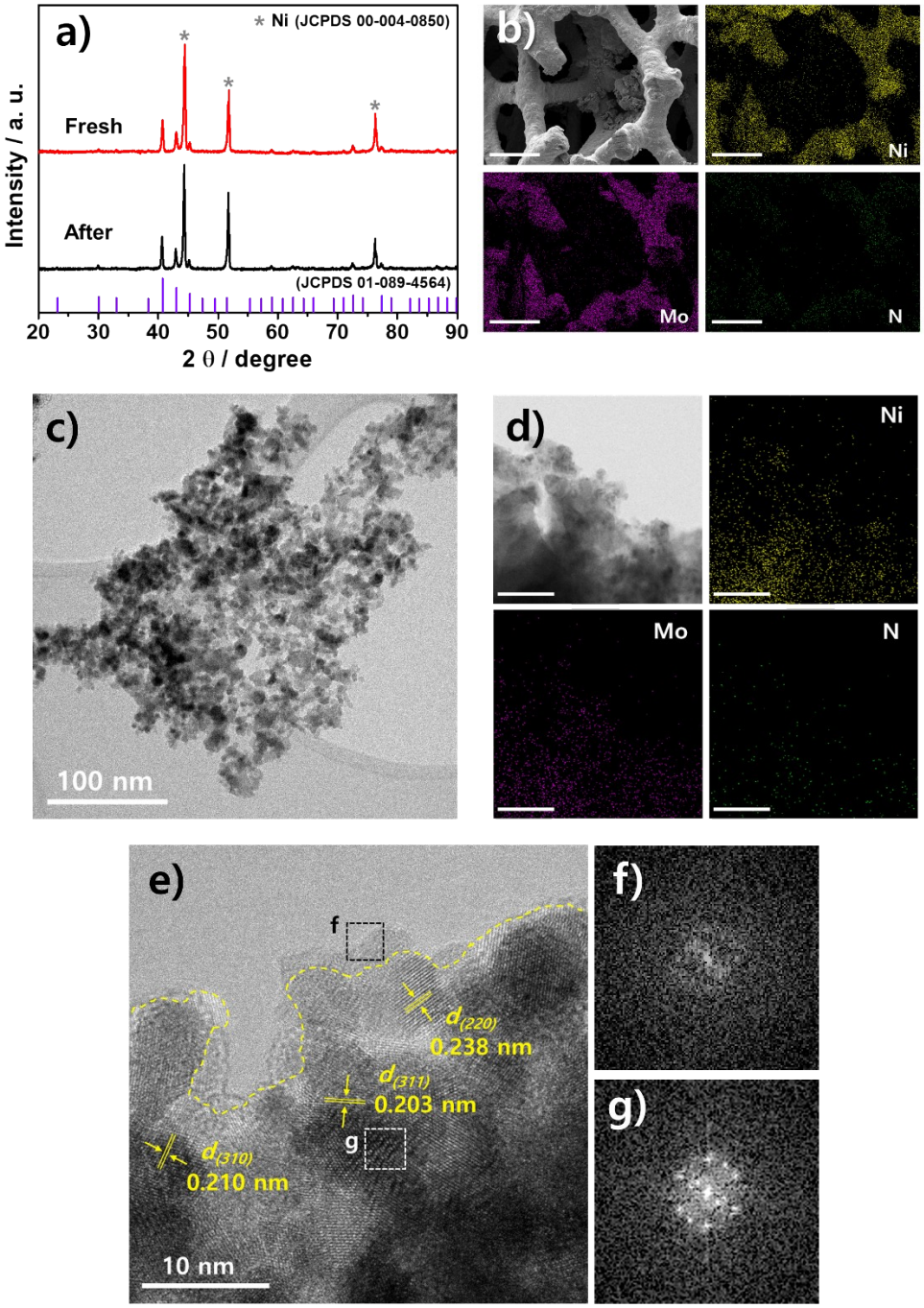

Fig. S9. (a) XRD patterns of Ni_2Mo_3N/NF fresh and after cycling tests. (b) SEM images of Ni_2Mo_3N/NF after cycling tests and corresponding SEM-EDS mapping for Ni, Mo, and N. Scale bar denotes 200 μm. (c) TEM images and (d) EDS mapping images of Ni, Mo, and N for Ni_2Mo_3N/NF after cycling tests. Scale bar denotes 50 nm. (e) HRTEM images of Ni_2Mo_3N/NF after cycling tests; (f), (g) FFT images.

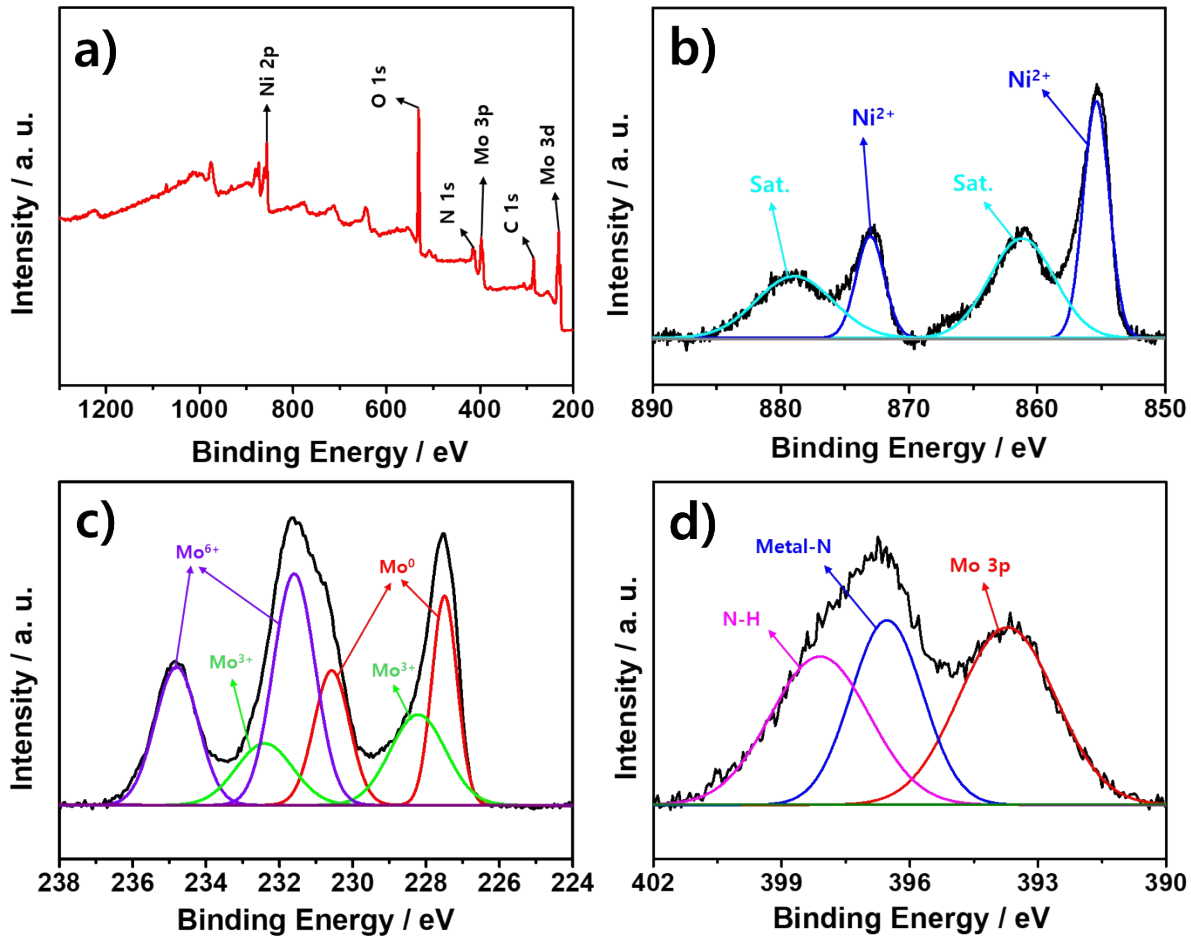

Fig. S10. XPS spectra of Ni_2Mo_3N/NF after cycling tests for (a) survey, (b) Ni 2p, (c) Mo 3d, and (d) N 1s.

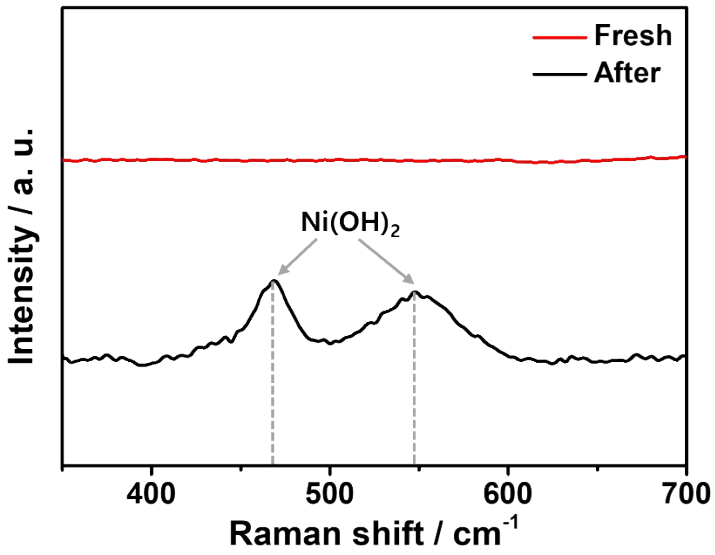

Fig. S11. Ex situ Raman spectra of Ni_2Mo_3N/NF fresh and after cycling tests.

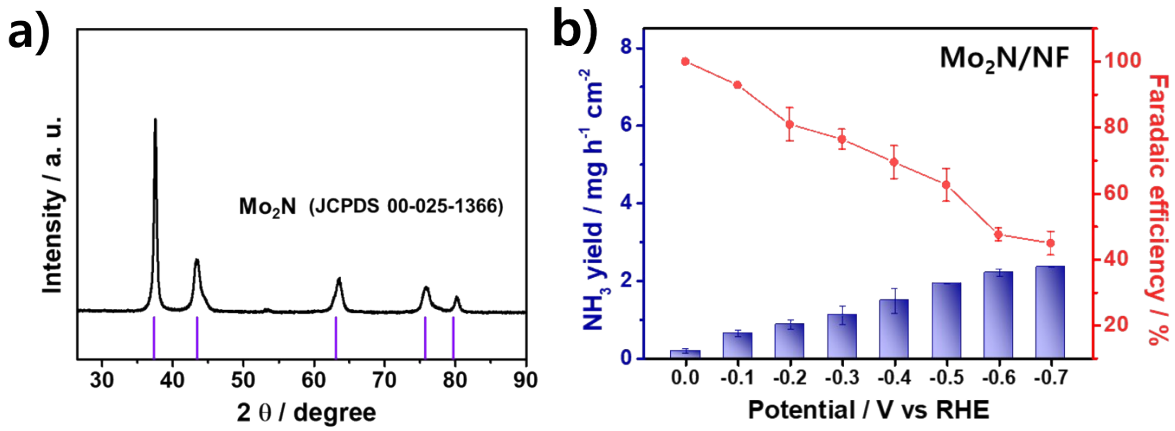

Fig. S12. (a) XRD pattern of the Mo_2N. (b) FE_{NH3} and NH_3 yield for Mo_2N/NF at different applied potentials.

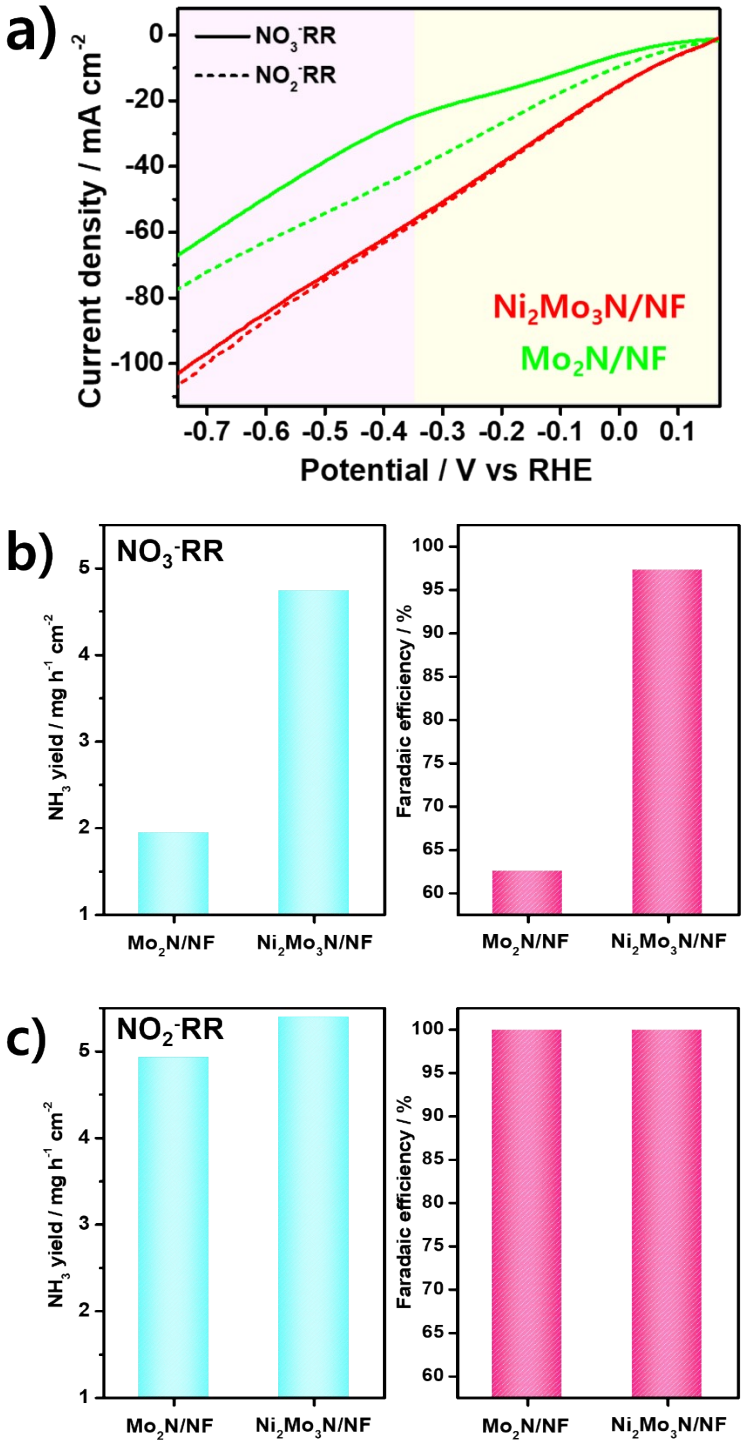

Fig. S13. (a) LSV curves for NO_3^-RR (solid line), NO_2^-RR (dashed line) on Ni_2Mo_3N/NF and Mo_2N/NF catalysts. (b) Comparison of NO_3^-RR performance between Ni_2Mo_3N/NF and Mo_2N/NF at -0.5 V vs RHE. (c) Comparison of NO_2^-RR performance between Ni_2Mo_3N/NF and Mo_2N/NF at -0.5 V vs RHE.

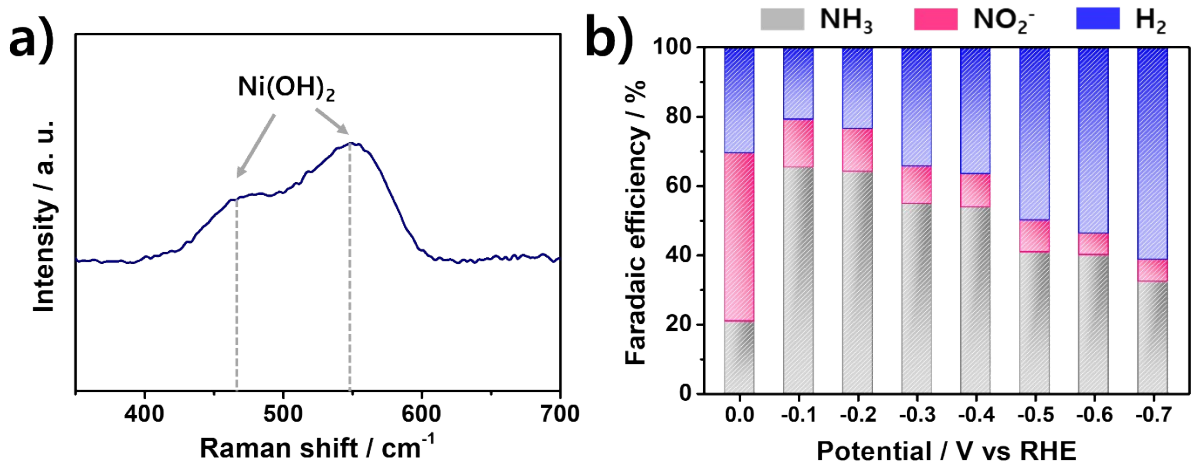

Fig. S14. (a) Ex situ Raman spectra of $Ni(OH)_2$/NF. (b) FEs of different products for $Ni(OH)_2$/NF after NO_3^-RR electrolysis under different conditions.

Table S1. Comparison of the electrochemical NO_3^-RR performance with Ni-, Mo-, and TMN-based electrocatalysts.

Electrocatalysts	Electrolytes	FE_{NH_3}	NH_3 yield	Ref.
Fe-MoS_2	0.1 M Na_2SO_4 + 0.1 M $NaNO_3$	98.0 % (@ -0.5 V)	0.51 mg h^{-1} cm^{-2} (@ -0.5 V)	1
Mo_2C/RGO	0.5 M Na_2SO_4 + 0.1 M $NaNO_3$	85.2 % (@ -0.6 V)	4.8 mg h^{-1} cm^{-2} (@ -0.6 V)	2
MoO_2/Ni	0.5 M K_2SO_4 + 0.1 M KNO_3	95.9 % (@ -0.3 V)	3.4 mg h^{-1} cm^{-2} (@ -0.3 V)	3
Cu-Ni	0.01 M KOH + 0.5 M Na_2SO_4	88.0 % (@ -1.0 V)	9.9 mg h^{-1} cm^{-2} (@ -1.2 V)	4
Ni_3B@$NiB_{2.74}$	0.1 M KOH + 0.1 M NO_3^-	98.7 % (@ -0.3 V)	3.3 mg h^{-1} cm^{-2} (@ -0.3 V)	5
$NiMoO_4$	0.5 M Na_2SO_4 + 0.05 M $NaNO_3$	96.1 % (@ -0.4 V)	2.2 mg h^{-1} cm^{-2} (@ -0.4 V)	6
MoO_2-C NBF	1 M KOH + 0.1 M KNO_3	99.0 % (@ -0.3 V)	1.8 mg h^{-1} cm^{-2} (@ -0.3 V)	7
$NiCoO_2$@Cu	0.1 M Na_2SO_4 + 0.1 M $NaNO_3$	94.2 % (@ -0.7 V)	5.9 mg h^{-1} cm^{-2} (@ -0.9 V)	8
FeMo-N-C	0.05 M PBS + 0.16 M KNO_3	94.7 % (@ -0.5 V)	0.3 mg h^{-1} cm^{-2} (@ -0.5V)	9
Cu_3N	0.1 M Na_2SO_4 + 0.1 M KNO_3	93.1 % (@ -0.6 V)	2.9 mg h^{-1} cm^{-2} (@ -0.6 V)	10
Cu_3N nanocube	0.1 M PBS + 0.1 M $NaNO_3$	76.0 % (@ -0.9 V)	2.0 mg h^{-1} cm^{-2} (@ -0.9 V)	11
Ni_2Mo_3N/NF	0.1 M KOH + 0.1 M $NaNO_3$	97.7 % (@ -0.5 V)	5.55 mg h^{-1} cm^{-2} (@ -0.7 V)	**This Work**

References

1. J. Li, Y. Zhang, C. Liu, L. Zheng, E. Petit, K. Qi, Y. Zhang, H. Wu, W. Wang, A. Tiberj, X. Wang, M. Chhowalla, L. Lajaunie, R. Yu and D. Voiry, *Adv. Funct. Mater.*, 2022, **32**, 2108316.
2. X. Li, S. Wang, G. Wang, P. Shen, D. Ma and K. Chu, *Dalton Trans.*, 2022, **51**, 17547-17552.
3. M. Fu, Q. Gou, Z. Ma, Y. Jiang, W. Shen, M. Li and R. He, *Appl. Surf. Sci.*, 2024, **643**, 158664.
4. Y. Bu, C. Wang, W. Zhang, X. Yang, J. Ding and G. Gao, *Angew. Chem. Int. Ed.*, 2023, **62**, e202217337.
5. L. Li, C. Tang, X. Cui, Y. Zheng, X. Wang, H. Xu, S. Zhang, T. Shao, K. Davey and S.-Z. Qiao, *Angew. Chem. Int. Ed.*, 2021, **60**, 14131-14137.
6. D. Li, J. Chen, S. Sun, C. Xu, Y. Sun, H. Mou, D. Wang and C. Song, *ACS Appl. Nano Mater.*, 2024, **7**, 13338-13346.
7. J. Yan, P. Liu, J. Li, H. Huang and W. Song, *Chem. Eng. J.*, 2023, **459**, 141601.
8. Y. Hai, X. Li, Y. Cao, X. Wang, L. Meng, Y. Yang and M. Luo, *ACS Appl. Mater. Interfaces*, 2024, **16**, 11431-11439.
9. E. Murphy, Y. Liu, I. Matanovic, S. Guo, P. Tieu, Y. Huang, A. Ly, S. Das, I. Zenyuk, X. Pan, E. Spoerke and P. Atanassov, *ACS Catal.*, 2022, **12**, 6651-6662.
10. J. Wei, G. Ye, H. Lin, Z. Li, J. Zhou and Y.-y. Li, *J. Colloid Interface Sci.*, 2024, **670**, 798-807.
11. P. Stein, H. Hall, R. Shimoni, N. E. Amitay, D. Bandyopadhyay, A. Neyman, R. Bar-Ziv and M. Bar Sadan, *ChemCatChem*, 2025, **17**, e202500156.